8-2019

Adsorption Driven Regolith-Atmospheric Water Vapor Transfer on Mars: An Analysis of Phoenix TECP Data

Holly Nicole Farris
University of Arkansas, Fayetteville

Adsorption Driven Regolith-Atmospheric Water Vapor Transfer on Mars: An Analysis of Phoenix TECP Data

A thesis submitted in partial fulfillment
of the requirements for the degree of
Master of Science in Space and Planetary Sciences

by

Holly Nicole Farris
Albion College
Bachelor of Arts in Physics, 2012

August 2019
University of Arkansas

This thesis is approved for recommendation to the Graduate Council.

Vincent Chevrier, PhD
Thesis Chair

John Dixon, PhD
Committee Member

Larry Roe, PhD
Committee Member

Mark Arnold, PhD
Committee Member

Edgard Rivera-Valentin, PhD
Ex-Officio Member

Abstract

NASA's Phoenix mission allowed for investigations of Martian diurnal water vapor cycles through the collection of temperature, relative humidity, and electric conductivity data by the Thermal and Electric Conductivity Probe (TECP) instrument. Using this data and previous experimental data, we propose a regolith-driven adsorption-desorption regime at the Phoenix landing site, where parameters intrinsic to the regolith are controlling localized relative humidity at the surface. To constrain these parameters, we model adsorption as a function of temperature and relative humidity across various Mars-relevant materials, defined by two layer-based adsorption theories: Langmuir (monolayer) and Brunauer-Emmett-Teller or BET (multilayer). Langmuir serves as an ideal adsorption model at high temperatures and low relative humidity, but diverges from the data at low temperature and high relative humidity (Martian night). Over these same values, BET continues to model the data once saturation of a monolayer is achieved. The BET model yielded fairly constant values for variables: volumetric surface coverage and enthalpy values, θ = 0.336, corresponding to 2.96 x 10^{-7} kg of H_2O/m^2 and ΔH = 52.783 +/- 1.206 kJ/mol, respectively. This occurred independent of material type. Holding these values constant, we then modeled an ideal BET adsorption coefficient, C = 89.4. Using our ideal BET adsorption coefficient, coupled with an "ideal" (observed by Viking 1) specific surface area, SSA = 1.7 x 10^4 m^2/kg, we conclude that the regolith at the Phoenix landing site is most likely a mixture mainly comprised of palagonitic material with properties similar to JSC Mars-1, which we bracket with a range of possible adsorption conditions. Ultimately, we explain adsorbed water content in the regolith at the Phoenix landing site and thus, adsorption, being driven by localized, diurnal variations in relative humidity.

Acknowledgements

I would like to acknowledge the funding that made this research possible. Portions of this work were supported by the National Aeronautics and Space Administration under Grant #NNX12AG67G issued through the Mars Fundamental Research Program and under Grant #NNX15AM42G issued through the Mars Data Analysis Program. This work was also made possible through the National Science Foundation "Research Experience for the Undergraduate" under Grant #1157002.

Thank you to my committee members, Dr. Vincent Chevrier, Dr. John Dixon, Dr. Larry Roe, Dr. Mark Arnold, and Dr. Edgard Rivera-Valentin for guidance, support, and collaboration throughout my graduate career. Thank you to Walter Graupner for technical support in the laboratory.

Thank you to Dr. Nicolle Zellner, Dr. Alfonso Davila, Dr. Rebecca Mickol, Dr. Erika Kohler, Julia Heydenreich, and Amanda Wagner for your support and friendship.

Thank you to Miguel Connor for a summer of hard work that contributed greatly to this thesis.

Dedication

This thesis is dedicated to my family and friends who support and inspire me.

My parents, Karen and Keith, my sister, Reilly, my husband, Andrew, and my friends, Meg and Heather, thank you for always being my biggest cheerleaders. Thank you all for sticking by my side and supporting me through the most stressful years of my life. I love you so much!

My late grandfather, James Stoddart, thank you for always encouraging me to look up at the stars and wonder where it all started.

Table of Contents

Chapter 1. Introduction 1

1.1 Water on Mars 1

1.2 Relevant Mars Missions 2

1.2.1 Viking I and II 3

1.2.2 Mars Odyssey 3

1.2.3 Phoenix 4

1.3 Adsorption 7

1.3.1. Langmuir Theory 7

1.3.2 Brunauer-Emmett-Teller (BET) Theory 8

1.4 Objective 9

Chapter 2. Methods 10

2.1 Phoenix TECP Data Analysis 10

2.2 Adsorption Modeling 12

Chapter 3. Results 15

3.1 BET Fit 15

3.2 Regolith Composition 19

Chapter 4. Discussion 21

Chapter 5. Conclusions 22

References 24

List of Tables

Table 3.1. BET adsorption parameters for various Mars-relevant materials. Surface coverage (θ) and enthalpy (ΔH) were modeled using the Origin 9.1 curve fitting function, resulting in a θavg = 0.336 ± 0.024 and ΔHavg = 52.783 ± 1.206 kJ/mol. Columns denoted with (*) show values obtained by Pommerol *et al.*, 2009 for reference.

Table 3.2. Ideal Martian regolith parameters conducive to adsorption include the specific surface area of actual Martian regolith reported from the Viking 1 landing site (1.7 x 10^4 m^2/kg) and the averaged modeled values obtained from the Origin 9.1 fit (Table 1). Three hypothetical regolith compositions and their inferred adsorption efficiency are included for comparison. *Model Regolith 1* depicts a regolith with adsorption efficiency closest to the *Ideal Regolith*, but with a large surface area. *Model Regolith 2* depicts a regolith with surface area closest to the *Ideal Regolith* and high adsorption efficiency. *Model Regolith 3* depicts a regolith with reasonable to large surface area, but very low adsorption efficiency.

List of Figures

Figure 1.1 Water ice material a few centimeters below the surface, exposed by the robotic arm on the Phoenix lander.

Figure 1.2 *Top*: Map showing brine stability where liquid water is possible with permanently frozen regions (grey), occasionally liquid (colored zones), and boiling zones (shaded zones with black lines). Brines are possible over the whole surface. High evaporation rates prevent long timescale stability on the surface. *Bottom:* A comparison between the distribution of nanophase ferric oxides as seen by the Mars Express OMEGA instrument (high abundance: white, low abundance: blue) and the humidity in the atmosphere, ranging from 0 (blue) to ~30 (red), as observed by the MGS-TES instrument in the equatorial regions. The similarity of both maps suggests the ferric oxides abundant in the regolith could control the atmospheric humidity through adsorption and desorption (Bandfield, 2002; Bibring *et al*., 2006).

Figure 2.1. Expected TECP T_b (board temperature) vs ln (R_H) slope as a function of temperature difference between the board and the real value. The slope does not change significantly for a reasonable temperature.

Figure 2.2. Phoenix TECP temperature and relative humidity data plotted beneath the frost lines for P_{sat} = 0.05 Pa (red, dashed) and P_{sat} = 0.2 Pa (green, dashed) for reference, Langmuir adsorption (blue), and BET adsorption (orange) consistent with parameters for JSC Mars 1. Phoenix temperatures vary, thus the adsorption lines are isochores (constant volumetric coverage), rather than isotherms (constant temperature).

Figure 3.1. Volumetric coverage (θ) plotted as a function of relative humidity for materials in Table 1 using BET adsorption theory. These are isotherms, T = 243 K (Beck *et al.*, 2010).

Figure 3.2. Phoenix TECP temperature and relative humidity data plotted with ideal BET (with averaged modeled values from Table 1) (yellow), BET with volumetric coverage (θ) increased by 75% (red), and BET with enthalpy (ΔH) increased by 75% (purple). The fit of the data is more dependent on an accurate value of θ, not ΔH, therefore, θ is assumed constant as a function of temperature.

Chapter 1. Introduction

1.1 Water on Mars

Since astronomer Giovanni Schiaparelli looked through his telescope and described the Martian surface as covered with canals in 1877, scientists have been fascinated with the fluvial history of the planet. Age dating of these fluvial features on the surface of Mars are divided into three categories, which roughly coincide with Mars' three epochs. The Noachian Era (3.8 - 3.5 Ga) is characterized by small valley networks and channels that originated as overflow of impact crater paleolakes, likely fed by precipitation. During the Hesperian Era (3.5 - 1.8 Ga), larger features appeared, such as large flood channels and "chaos terrain" (Coleman and Baker, 2009), areas of collapse fueled by the release of pressurized groundwater. Lastly, the Amazonian Era (1.8 Ga - present) is characterized by small channels and glacial features. Glacial features, located in the mid-latitudes, particularly around the Tharsis Bulge, formed around the time of Olympus Mons. This suggests a very different climate in Mars' recent past (Head *et al.*, 2006). While still wildly debated, most believe these older terrains provide evidence for a previously warmer and wetter Mars. For example, valley networks and glacial features provide evidence for and indicate a more energetic hydrological cycle in the past. Currently, almost all water at the surface is bound as ice, except for transient melting of ice, occurring as depressions, gullies (Malin and Edgett, 2000; Hecht, 2002), and/or potentially, recurring slope lineae (Levy, 2012). Melting of transient ice occurs preferentially at mid to high latitudes, on pole-facing slopes, and likely in the presence of hygroscopic salts, such as perchlorates (Zorzano *et al*., 2009; Chevrier *et al.*, 2009, Ohja *et al., 2015*).

The ice caps, present at both poles, are predominantly composed of water ice and carbon dioxide ice. Due to Mars' axial tilt, it has seasons similar to Earth. During the winter, CO_2

freezes out of the atmosphere and accumulates on the ice caps. In the summer, the CO_2 ice sublimates away, exposing the water ice beneath it to solar insolation. The subsequent seasonal transport of water vapor gives rise to frost and clouds (Mellon *et al.*, 2003).

Current Mars is a cold, hyper-arid desert with average conditions (temperature, pressure, etc.) below the triple point of water (Marchant and Head, 2007). However, due to variations in orbital parameters (Laskar, *et al.*, 2004), ice is generally not stable at equatorial and mid-latitude regions (Mellon and Jakosky, 1995). Consequently, there exist microenvironments where liquid water is metastable at the surface for several hours to days at a time throughout the Martian year (Haberle *et al.*, 2001; Lobitz *et al.*, 2001). These environments are concentrated in regions that allow melting of surface or near-surface ice, like impact crater basins or in the presence of certain soil chemistries (Chevrier *et al.*, 2009), that rapidly evaporate/diffuse, adsorb/desorb, or freeze. In fact, fluvial erosion occurring from the Late Amazonian to the present only accounts for a tiny fraction of Mars' total fluvial activity.

1.2 Relevant Mars Missions

The majority of the information concerning Mars comes from orbital and ground-based observations, direct imaging, mission data collected by spacecraft, and subsequent analyses such as geochemical mapping and global circulation models (GCMs). In the search for life beyond Earth, space agencies turn to Mars for many reasons; including its proximity/accessibility and interesting fluvial history and soil chemistry. Liquid water is the key requisite of life as we know it, therefore, most missions to Mars include a "water-centric" instrument in its payload.

1.2.1 Viking I and II

Viking I and II were identical spacecraft each consisting of an orbiter and a lander that landed on Mars on August 20, 1975 and September 9, 1975, respectively. The Viking missions were designed to characterize the composition of the atmosphere and surface of Mars, while looking for possible life and conducting a series of biology experiments at Mars' mid latitudes. These biology experiments were successful in identifying agents in the soil which were the result of chemical weathering of silicates by low-temperature frost and adsorbed water (Huguenin, 1982). The Martian regolith was determined to be mostly an assemblage of magnesium and sodium sulfates, sodium chloride, magnesium and calcium carbonates (Clark and Van Hart, 1981), and smectite clays (Banin and Rishpon, 1979). Additionally, the Mars Atmosphere Water Detector (MAWD) experiments reported water vapor content abundances in the atmosphere between 0 and 100 precipitable microns (pr μm), depending on location and season. Futhermore, the annual global distribution of water vapor in the atmosphere correlates well with Martian topography, surface albedo, and thermal inertia, thus controlled by the surface and subsurface on adsorption/desorption processes (Jakosky and Farmer, 1982).

1.2.2 Mars Odyssey

Mars Odyssey reached Mars' orbit on October 24, 2001. The THEMIS (Thermal Emission Imaging System) instrument globally mapped the amount and distribution of various chemical elements at the Martian surface (Christensen *et al*., 2003; Christensen *et al.*, 2004). By 2008, it had mapped hydrogen distribution across the Martian surface, leading scientists to discover large quantities of water ice bound as ice caps in the polar regions and buried just

beneath the surface in mid to high latitudes (Boynton *et al.*, 2002; Mellon *et al.*, 2009; Smith *et al.*, 2009), which was directly detected, later, by the Phoenix lander (Fig 1.1).

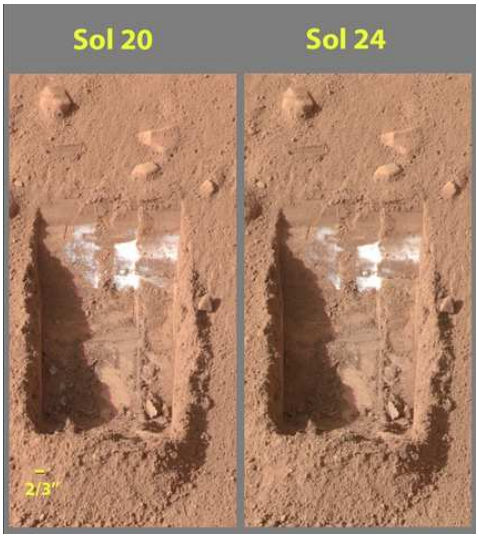

Figure 1.1 Water ice material a few centimeters below the surface, exposed by the robotic arm on the Phoenix lander (Hecht *et al*., 2009).

1.2.3 Phoenix

NASA Phoenix landed in the North Polar Region of Mars on May 25, 2008. The landing site, Vastitias Borealis (68.2 N, 234.3 E), is a polar region characterized by near-surface ice. Perhaps the most significant finding from the Phoenix mission was the detection of 0.4 to 0.6 wt% perchlorate (ClO_4) in the Martian soil (Hecht *et al.*, 2009), of which are dominated by $Mg(ClO_4)_2$ and $Ca(ClO_4)_2$, consistent with weathering of magnesium and calcium carbonates (Kournaves *et al.*, 2014). Additionally, Phoenix directly detected subsurface water ice and contributed vastly to our further understanding of Martian climate and soil chemistry, specifically that the stability of subsurface water ice is largely due to the thermal and diffusive properties of the regolith. The Phoenix mission was the first time a detailed investigation of the diurnal water cycle on Mars could be conducted (Pommerol *et al.*, 2009; Chevrier *et al.*, 2008)

through the collection of temperature, relative humidity, and electric conductivity data using the TECP (Thermal and Electric Conductivity Probe) instrument (Zent *et al.*, 2009). Previously, regolith parameter control of local relative humidity through the adsorption and desorption of atmospheric water vapor had only been proposed through Mars Express OMEGA data analyses (Fig 1.2).

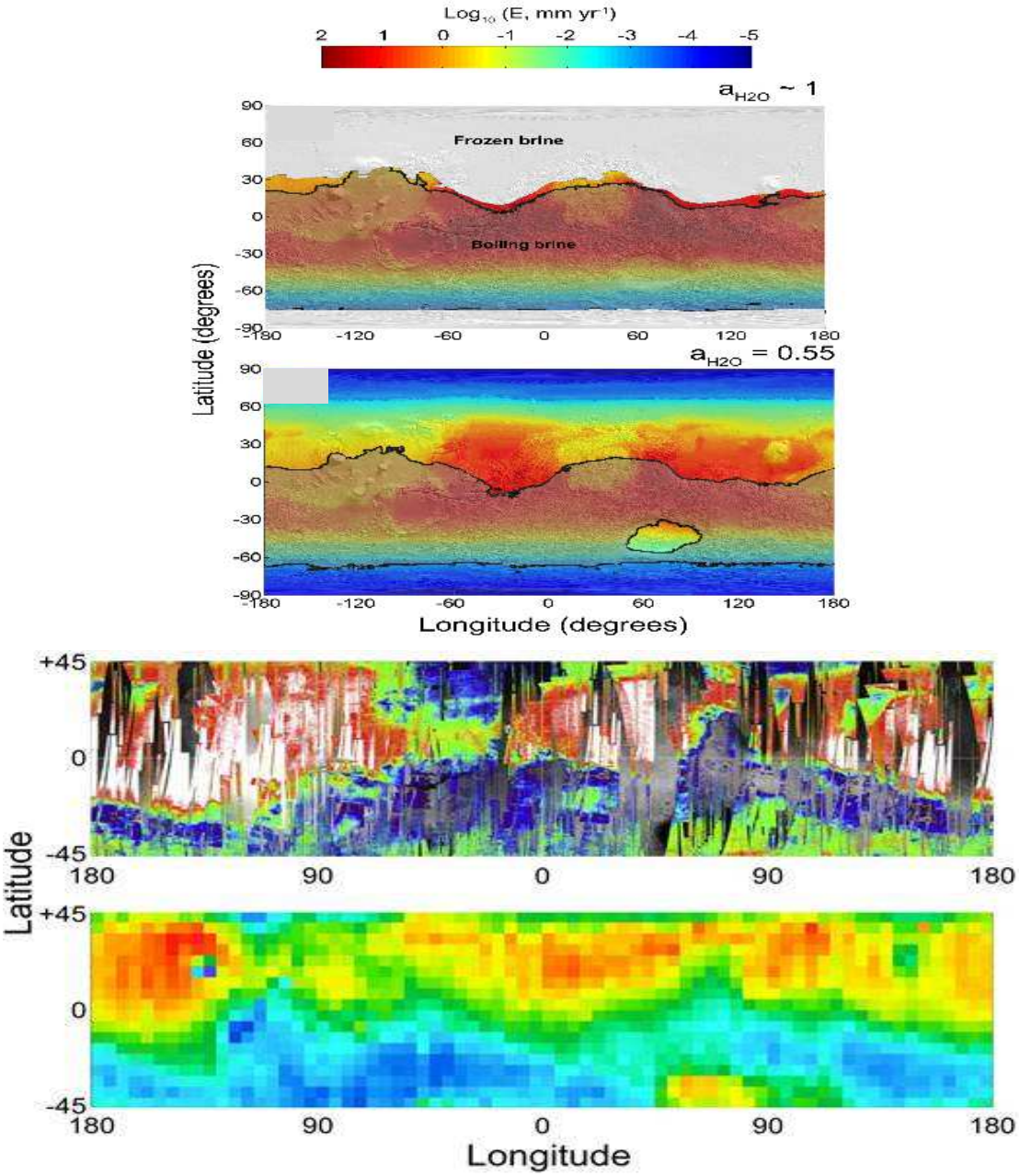

Figure 1.2 *Top*: Map showing brine stability where liquid water is possible with permanently frozen regions (grey), occasionally liquid (colored zones), and boiling zones (shaded zones with black lines). Brines are possible over the whole surface. High evaporation rates prevent long timescale stability on the surface. *Bottom:* A comparison between the distribution of nanophase ferric oxides as seen by the Mars Express OMEGA instrument (high abundance: white, low abundance: blue) and the humidity in the atmosphere, ranging from 0 (blue) to ~30 (red), as observed by the MGS-TES instrument in the equatorial regions. The similarity of both maps suggests the ferric oxides abundant in the regolith could control the atmospheric humidity through adsorption and desorption (Bandfield, 2002; Bibring *et al*., 2006).

1.3 Adsorption

Physical adsorption assumes an atomically flat surface that is exposed to a vapor, in our case water vapor, held at a pressure, *P*, and a temperature, *T*. Gas molecules incident upon the surface, in general, do not rebound, but rather condense on it. The molecules are held or adsorbed on the surface by forces similar to those holding together the atoms of a molecule. When these forces are strong enough, the rate of evaporation may be so slow that adsorbed molecules cover the surface. In simplest terms, when *P* is low and *T* is high, the number of molecules per unit area on the surface is small. As *P* increases and/or *T* decreases, we can image a variety of evolutions of film structures on the surface (Bruch *et al.*, 1997). This behavior is most frequently expressed through one of two layer-driven theories: Langmuir and BET.

1.3.1. Langmuir Theory

The simplest study of adsorption assumes a single film lattice model, where a surface consists of an array of N_s possible, identical adsorption sites. Using the ideal gas law (Eqn. 1.1):

$$P = \frac{n}{\beta} = \frac{nk_BT}{v} \qquad (1.1)$$

where *P* is pressure, *n* is the number density of the vapor (N/N_s), k_B is the Boltzmann constant, and *T* is temperature. The Langmuir isotherm (Eqn. 1.2) is then expressed fractionally as:

$$\theta = \frac{N}{N_s} = \frac{P}{(P+P_L)} \qquad (1.2)$$

This indicates that the coverage of the vapor molecules on the surface rises linearly at values of *P* that is much greater than P_L, according to Henry's Law (assumes a linear relationship between

coverage and pressure), where P_L is the pressure at a given T at which $\theta = ½$. Coverage reaches saturation as $N \rightarrow N_s$ or 1. Every site, N_s, is occupied and a monolayer of one molecular thickness (3×10^{-10} m) is achieved. The number of gas molecules cannot exceed N_s. The forces acting between two layers of gas molecules will usually be much less than those between the solid surface and the first layer of molecules. The rate of evaporation from a potential second layer is much more rapid than the first, so when a molecule strikes a portion of the surface already covered with a monolayer, it will evaporate quickly and is therefore negligible (Langmuir, 1918; Bruch *et al.*, 1997).

1.3.2 Brunauer-Emmett-Teller (BET) Theory

Brunauer-Emmett-Teller (BET) is an extension of the Langmiur Theory, which applies to multilayer film model, where particles are allowed to occupy a three-dimensional array of sites above a surface (Brunauer *et al*., 1938). Per Equation 1.1, Langmuir assumes n = 1, BET assumes n = ∞. The BET isotherm (Eqn. 1.3) is expressed as:

$$\frac{xN_s}{(1-x)N} = \frac{[1+x(c-1)]}{c} \qquad (1.3)$$

Where x is the ratio of the pressure to the saturated pressure (the value at which N diverges) and c is a constant. To determine the surface coverage, N is measured as a function of x so as to deduce the unknowns, N_s and c (Brunauer *et al.*, 1938; Bruch *et al.*, 1997).

1.4 Objective

While diffusion can explain liquid water stability over long timescales (periods of high obliquity), it is the dynamics of water vapor at short timescales (day to year), which remain unknown. Local effects, mostly related to the phase changes of water, including adsorption (Chevrier *et al.*, 2008), formation of liquid (Sears and Moore, 2005), and interaction with hygroscopic salts through hydration, deliquescence, and dissolution (Chevrier and Altheide, 2008; Chevrier *et al.*, 2009; Sears and Chittenden, 2005) can all be attributed to the transient variations in water vapor dynamics. Using Phoenix TECP data, we propose an evaporation-adsorption cycle, where water alternates between thin layers on the surface of porous regolith and as water vapor in the atmosphere. This suggests regolith parameters, such as specific surface area, may influence atmospheric humidity through adsorption and desorption (Jakosky *et al.*, 2005; Pommerol *et al.*, 2009; Zent *et al.*, 1997; Zent *et al.*, 2001; Chevrier *et al.*, 2008; Bryson *et al.*, 2008). Langmuir and BET adsorption theories are implemented to explain sol-to-sol dependencies between temperature, humidity, and regolith parameters at the Phoenix landing site and thus, the implications for transient, adsorbed, liquid water at the surface.

Chapter 2. Methods

2.1 Phoenix TECP Data Analysis

The dataset used for this study is the most current Phoenix TECP data, per the revised calibration function present by Zent *et al.*, 2016 and was obtained from V. F. Chevrier, a co-author of the publication. Phoenix TECP measured relative humidity, *RH*, using a capacitance-based relative humidity sensor, located above the TECP needles. Saturation vapor pressure, P_{sat}, was calculated using the board temperature, T_b, measured using a Type E thermocouple located near the humidity sensor (Smith *et al.*, 2008; Zent *et al.*, 2009). Computing the vapor pressure at the frost point temperature allowed for the calculation of the pressure of water, P_{H2O}. Using these two calculations, *RH* could then be found and plotted as a logarithmic function against the temperature (Fig. 2.1).

$$RH = \frac{P_{H_2O}}{P_{sat}} \qquad (2.1)$$

It is important to note that the TECP measured temperature and relative humidity both in the soil and atmosphere, where air measurements were obtained between 0.14 m and 2.3 m while in-soil measurements are integrated over the length of the TECP needles, 15 mm, and therefore are affected by the steep regolith temperature gradient (Zent et al., 2010). Additionally, because of the location of the humidity sensor, during some in-soil *T* measurements, *RH* was measured in-air. However, most of the TECP measurements were made in-air (~80%) (Rivera-Valentin and Chevrier, 2015). To determine the possible effect of the varied measurements on our analysis, we studied the slope of data in T_b and *RH* space using a least-squares fit to 95% confidence. We find that the slope using all of the data is -8.7 ± 0.3 while using only in-air measurements provided a slope of -9.0 ± 0.1; both values are statistically indistinguishable.

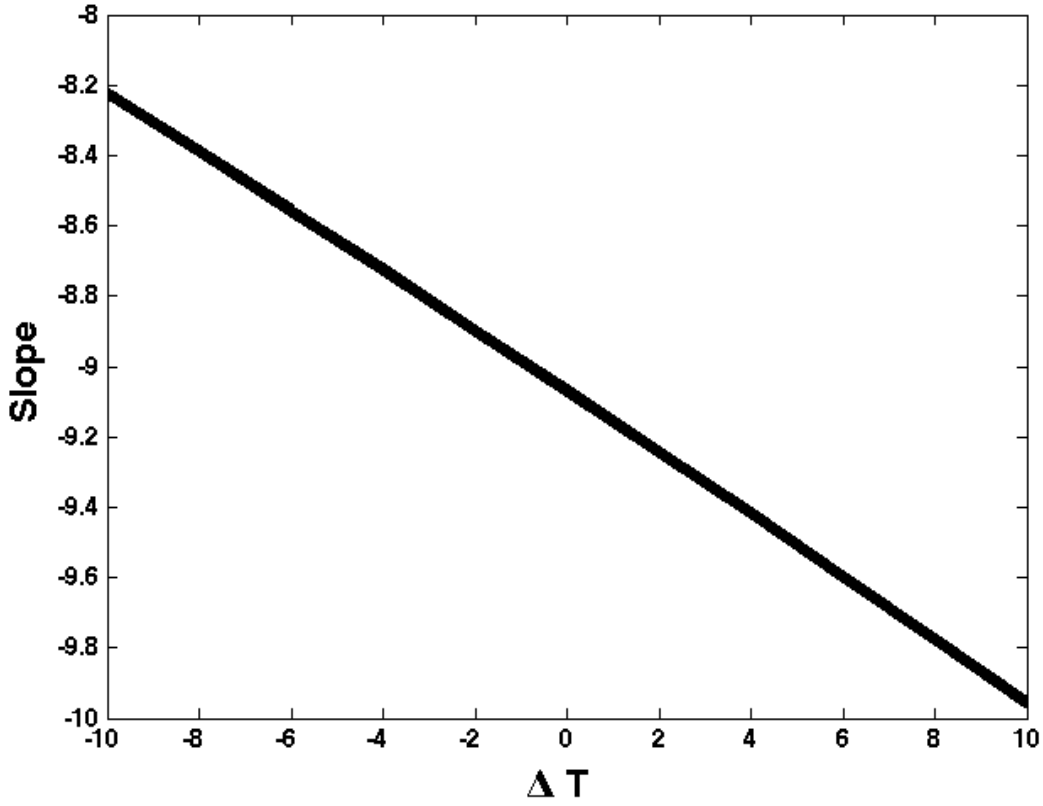

Figure 2.1. Expected TECP T_b (board temperature) vs ln (R_H) slope as a function of temperature difference between the board and the real value. The slope does not change significantly for a reasonable temperature.

Figure 2.1 shows the expected T_b vs ln(RH) slope as a function of temperature difference between the board and the real value. For example, a slope change of around 0.2 corresponds to about a 2 K difference in temperature (Rivera-Valentin and Chevrier, 2015). Moving forward, we use all the TECP data in order to improve our number statistics.

2.2 Adsorption Modeling

Adsorption depends upon several properties of the regolith, such as the adsorption coefficient (C), surface coverage (θ), and specific surface area (SSA), as well as enthalpy (ΔH), which varies with regolith. The adsorption coefficient is a dimensionless constant representative of the efficiency at which molecules, in this case water, adsorb at a surface. Surface coverage is another dimensionless value, which describes the fractional surface area (Langmuir) or surface volume (BET) covered by water. Enthalpy, measured in kJ/mol, is defined as the difference between heat of adsorption and heat of liquefaction. Since adsorption decreases the surface energy of the adsorbent, it is always exothermic, and therefore, ΔH is always negative. Lastly, the specific surface area, SSA, of a material is measured in m^2/kg and describes a total surface area by unit mass. The SSA is useful in understanding the particle size distribution and texture of a material. Isolating each parameter one at a time will allow us to understand how each affects the readiness of various regolith simulants at Phoenix landing site conditions to adsorb water and in what quantities.

Here we applied the Langmuir and BET models. In the Langmuir theory, the vapor pressure of water, P_{H2O}, is given by the following equation (Eqn 2.2) or in terms of relative humidity as Equation 2.3.

$$P_{H_2O} = \frac{\theta}{\alpha(1-\theta)} \qquad (2.2)$$

$$RH = \frac{\theta}{C-C\theta} \qquad (2.3)$$

where θ is the surface coverage (the fraction of the surface covered by water) and α is the Langmuir thermodynamic adsorption constant. C, the adsorption coefficient, is a constant that is

defined as $C = \alpha P_{sat}$. The temperature dependency of α is given by the following equation (Eqn 2.4)

$$\alpha = \alpha_0 \frac{P_{sat}(T_0)}{P_{sat}(T)} \, exp\left[-\frac{\Delta H}{R}\left(\frac{1}{T} - \frac{1}{T_0}\right)\right] \qquad (2.4)$$

where R is the ideal gas constant (~8.314 $Jmol^{-1}K^{-1}$), T is temperature, ΔH is enthalpy, defined as the difference between heat of adsorption and heat of liquefaction, and P_{sat} (T) is the saturation pressure at temperature T. Starting with a reference α_o value, α can be calculated for any other temperature. The two remaining variables, θ and ΔH are varied to best fit the data.

The BET approach is analogous. Rearranging the BET equation and solving for RH (Eqn. 2.5) gives:

$$RH = \frac{-C-2\theta+C\theta+\sqrt{C}\sqrt{C+4\theta-2C\theta+C\theta^2}}{2\theta(C-1)} \qquad (2.5)$$

Here, θ is the volumetric coverage and again, C is the adsorption coefficient that can also be expressed as Equation 2.6.

$$C = C_0 exp\left[-\frac{\Delta H}{R}\left(\frac{1}{T} - \frac{1}{T_0}\right)\right] \qquad (2.6)$$

To determine which theory more accurately follows the trend seen in the data, no constraints were placed on the variables. Rather, the θ and ΔH parameters were varied to find a best fit of the data. Theoretical Langmuir, BET, and frost (P_{H2O} = 0.2 Pa and P_{H2O} = 0.05 Pa) lines were plotted against the Phoenix TECP temperature and relative humidity data (Fig. 2.2). There is a divergence between the data and Langmuir, particularly at high relative humidities and low temperatures (typical of Martian night).

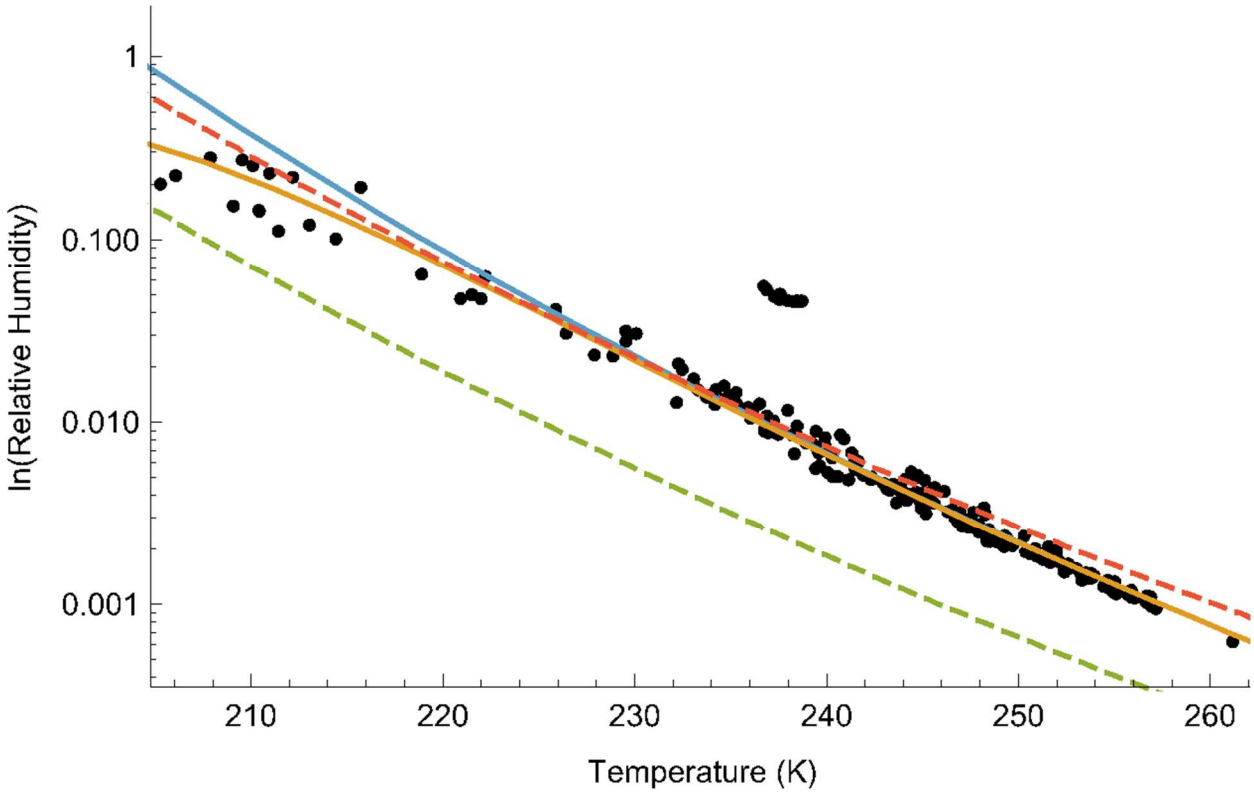

Figure 2.2. Phoenix TECP temperature and relative humidity data plotted beneath the frost lines for P_{sat} = 0.05 Pa (red, dashed) and P_{sat} = 0.2 Pa (green, dashed) for reference, Langmuir adsorption (blue), and BET adsorption (orange) consistent with parameters for JSC Mars 1. Phoenix temperatures vary, thus the adsorption lines are isochores (constant volumetric coverage), rather than isotherms (constant temperature).

Over these same values, BET provides a closer fit of the data. Since Langmuir only accounts for a monolayer, once saturation is reached, BET becomes the favored model of adsorption, despite the low water pressure on Mars.

Chapter 3. Results

3.1 BET Fit

Using Origin 9.1, a scientific graphing and data analysis program, we fit the BET adsorption function to the Phoenix TECP data using experimentally derived adsorption coefficient values from Pommerol et al., 2009 for JSC-Mars 1, ferrihydrite, smectite, dunite, volcanic tuff, and volcanic tuff + magnesium sulfate mixture (Table 2.1). The Origin 9.1 package includes an advanced curve-fitting function, which fits a complex data set employing a user-defined function. First, the function is defined by entering Equations 2.4 and 2.5 where relative humidity is given as a function of temperature, adsorption coefficient, enthalpy, and surface coverage. For each simulant, the adsorption coefficient value from Pommerol *et al.*, 2009 was fixed, while enthalpy and volumetric coverage were left unfixed and allowed to vary freely. We ran the fitting function and report the resulting values and corresponding errors in Table 3.1 along with Pommerol, *et al*., 2009 values for reference. It is important to note that a BET fit using the parameters for each regolith simulant shows volumetric coverage (θ_{BET}) varying as a function of relative humidity (*RH*). These represent isotherms, as all experiments were conducted at a constant temperature, T = 243 K (Fig. 3.1). Volumetric coverage and enthalpy do not vary greatly as a function of most materials and since Phoenix temperatures vary, this is indicative of an isochore, per Figure 2.2 and 3.2, respectively. A BET fit of the data with enthalpy increased by 75%, does not affect the trend of the fit. Therefore, volumetric coverage and enthalpy results were averaged, producing "ideal" values for regolith at the Phoenix landing site, 0.336 ± 0.024 and 52.783 ± 1.206 kJ/mol, respectively. Using these values, we solve for an ideal BET adsorption coefficient, C_{ideal}.

Table 3.1. BET adsorption parameters for various Mars-relevant materials. Surface coverage (θ) and enthalpy (ΔH) were modeled using the Origin 9.1 curve fitting function, resulting in a $\theta_{avg} = 0.336 \pm 0.024$ and $\Delta H_{avg} = 52.783 \pm 1.206$ kJ/mol. Columns denoted with (*) show values obtained by Pommerol *et al.*, 2009 for reference.

Material	θ*	θ	C*	ΔH* (kJ/mol)	ΔH (kJ/mol)	T* (K)	SSA* (m^2/kg)
JSC Mars 1	0.329	0.37 ± 0.004	103.4 ± 8.4	52.6	49.952 ± 1.372	243	1.06×10^5
Ferrihydrite	0.211	0.25 ± 0.02	56 ± 8.5	53.9	51.703 ± 1.262	243	1.34×10^5
Smectite (SWy-2)	0.027	0.04 ± 0.03	5.7 ± 0.9	57.4	52.945 ± 1.185	243	5.27×10^4
Dunite	0.362	0.4 ± 0.03	120.8 ± 3.0	55.0	53.343 ± 1.172	243	2.83×10^3
Volcanic Tuff	0.41	0.45 ± 0.03	149.4 ± 48.4	55.5	53.945 ± 1.143	243	1.37×10^4
Tuff/Mg-Sulfate	0.474	0.51 ± 0.03	196 ± 82.9	57.2	54.812 ± 1.103	243	1.13×10^4
Average	**-**	**0.336 ± 0.024**	**-**	**-**	**52.783 ± 1.206**	**-**	**-**

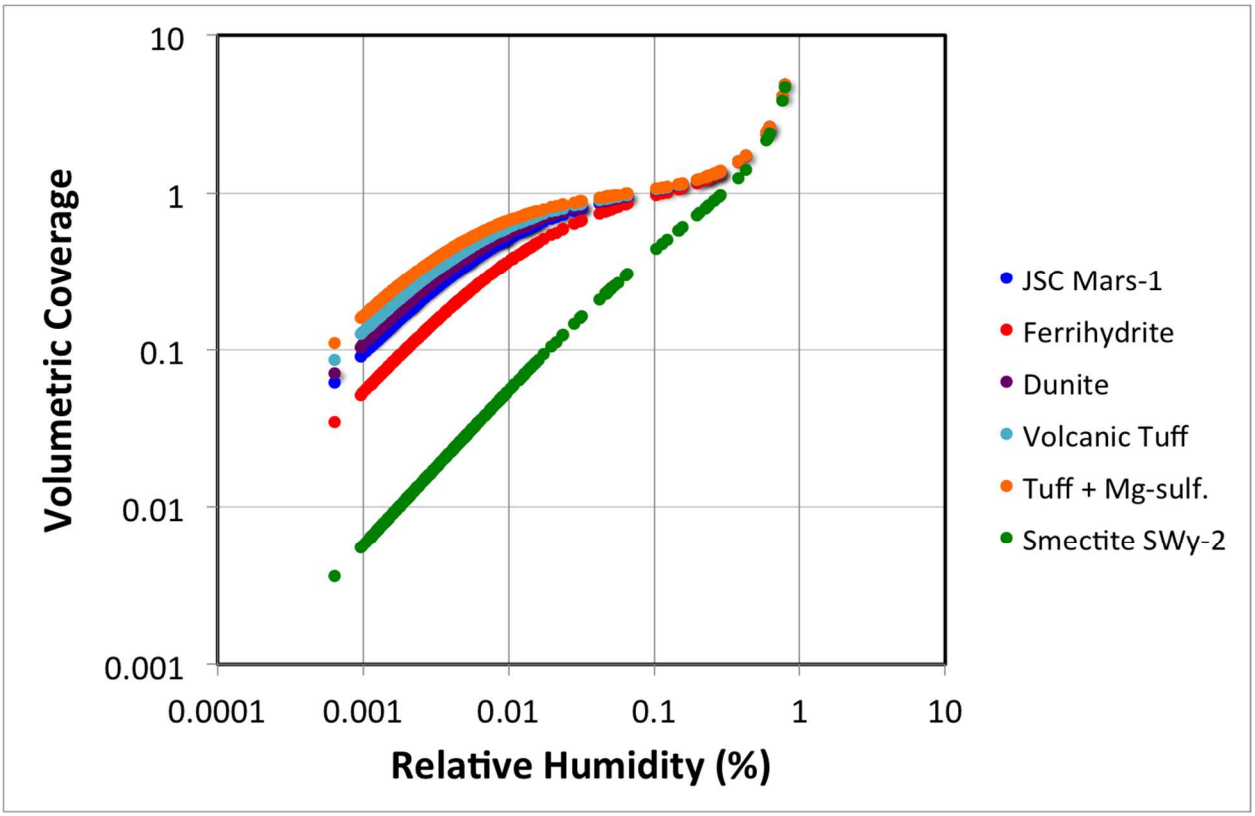

Figure 3.1. Volumetric coverage (θ) plotted as a function of relative humidity for materials in Table 1 using BET adsorption theory. These are isotherms, T = 243 K (Beck *et al.*, 2010).

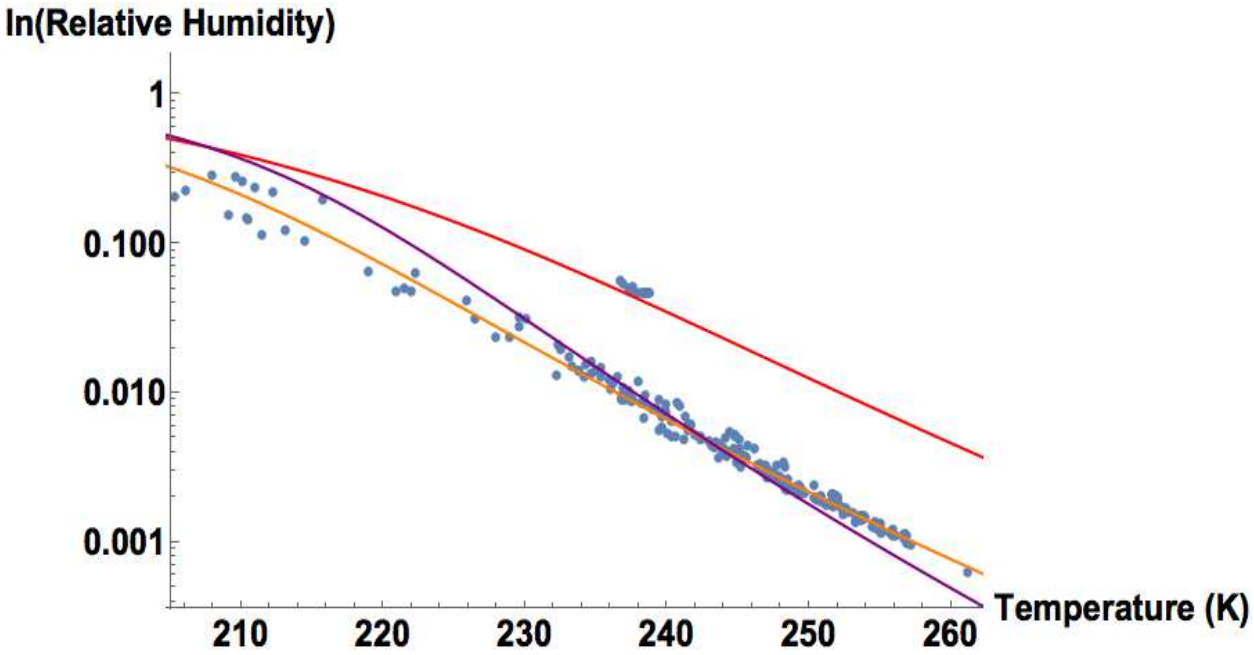

Figure 3.2. Phoenix TECP temperature and relative humidity data plotted with ideal BET (with averaged modeled values from Table 1) (yellow), BET with volumetric coverage (θ) increased by 75% (red), and BET with enthalpy (ΔH) increased by 75% (purple). The fit of the data is more dependent on an accurate value of θ, not ΔH, therefore, θ is assumed constant as a function of temperature.

3.2 Regolith Composition

Our modeled ideal BET adsorption coefficient, presented in Table 3.2 is C_{ideal} = 89.4. This value falls near the median of the range of reported values in the literature but does not correspond to any one material, meaning adsorption is occurring in a regolith that is a mixture. For example, a regolith composed of 100% dunite has a small specific surface area of 2.83 x 10^3 m^2/kg (compared with 1.7 x 10^4 m^2/kg reported at the Viking I landing site (Ballou *et al*., 1978)), and an adsorption coefficient, 120.8, suggesting an adsorption rate too efficient to be realistic under Martian conditions. Conversely, a regolith composed of 100% ferrihydrite has a specific surface area (1.34 x 10^5 m^2/kg) much larger than what is seen on Mars and an adsorption coefficient, 56.5, suggesting an inefficient adsorption rate to describe the observations at the Phoenix landing site. Though both of these materials are ubiquitous on Mars, it is clear that a homogeneous regolith regime is not ideal for adsorption/desorption cycles at the surface. However, a hypothetical regolith composed of 50% dunite and 50% ferrihydrite has a specific surface area of 3.56 x 10^4 m^2/kg, roughly twice the Viking I value, and an adsorption coefficient of 104.7, compared with C_{ideal} = 89.4 (Table 3.2). In this instance, a simple 1:1 binary mixture of two know materials on Mars yields a better specific surface area and adsorption coefficient, than either of the materials would on their own.

Table 3.2. Ideal Martian regolith parameters conducive to adsorption include the specific surface area of actual Martian regolith reported from the Viking 1 landing site (1.7×10^4 m^2/kg) and the averaged modeled valued obtained from the Origin 9.1 fit (Table 3.1). Three other hypothetical regolith compositions and their inferred adsorption efficiency are also included for comparison. *Model Regolith 1* depicts a regolith with adsorption efficiency closest to the *Ideal Regolith*, but with a large surface area. *Model Regolith 2* depicts a regolith with surface area closest to the *Ideal Regolith* and high adsorption efficiency. *Model Regolith 3* depicts a regolith with reasonable to large surface area, but very low adsorption efficiency.

	Ideal Regolith	**Model Regolith 1**	**Model Regolith 2**	**Model Regolith 3**
Composition	Viking I Site	50% JSC Mars 1 50% Ferrihydrite	75% Dunite 25% Ferrihydrite	100% Smectite (SWy-2)
θ	0.336	0.336	0.336	0.336
ΔH (kJ/mol)	52.783	52.783	52.783	52.783
C_{model}	89.4	89.4	89.4	89.4
SSA (m^2/kg)	1.7×10^4	1.2×10^5	3.56×10^4	9.0×10^4
Actual C	-	80	104.7	5.7
Actual C (±) (%)	-	10.5	17.1	93.6

In Table 3.2, two other hypothetical binary mixtures are investigated, bracketing a range of possible adsorption conditions. With adsorption possible over such a range, this implies adsorption could be occurring at various latitudes with various regolith compositions depending on the temperature and relative humidity, and therefore, season and time of day.

Chapter 4. Discussion

The Phoenix TECP data was fit with Langmuir and BET adsorption curves, as well as compared to the frost line. Despite low temperatures, frost formation is not driving diurnal cycles in relative humidity at the Phoenix landing site. Rivera-Valentin and Chevrier, 2015 argue that frost formation could explain this data. Their work shows humidity data binned and averaged over 1-hour intervals as a function of water vapor pressure. Most of the data centers on P_{H2O} = 0.2 Pa, one value used to calculate a frost line plotted in Figure 3.2. This frost line does not overlap the TECP data, so an additional frost line was added for comparison (P_{H2O} = 0.05 Pa); P_{H2O} mimics the pressure drop we would expect to see at night, which appears to describe the data well, however not at low temperatures. At saturation pressure, the frost line is indistinguishable from Langmuir and we expect to always have frost, however, there are very few observations of physical, wide spread frost at the Phoenix landing site (Smith *et al*., 2009). At night, when temperature and pressure drop, this could possibility be due to frost (Rivera-Valentin and Chevrier, 2015), but Phoenix data is collected over Mars' summer months and it is possible these are frost-free times of the year (Cull *et al.*, 2010). Therefore, adsorption, coupled with the cohesive nature of the regolith at the Phoenix landing site, serves as an active water vapor sink in the regolith (Smith *et al.,* 2009; Arvidson *et al.*, 2009; Rivera-Valentin and Chevrier, 2015).

Chapter 5. Conclusions

Modeling BET adsorption of the data across Mars-relevant materials yielded values consistent with previous studies reported in the literature (Beck *et al.*, 2010; Pommerol *et al.*, 2009; Chevrier *et al.,* 2008, and Bryson *et al.,* 2008), with an average surface coverage achieved, θ = 0.336, corresponding to 2.96 x 10^{-7} kg of H_2O/m^2. We explain volumetric coverage of adsorbed liquid water remaining fairly constant across regolith composition by looking at the water distribution across the planet. Most of the water on Mars is locked up in the dominant phase of ice, mainly comprising the polar caps, the density of which is poleward of +/- 60 latitude, as mapped by the Mars Odyssey Neutron Spectrometer (Feldman *et al.*, 2002 and Mitrofanov *et al.*, 2002). Ultimately, there is very little condensable water vapor in the atmosphere, simply not enough to adsorb large quantities of water onto the surface. If this water were deposited onto the surface, it would cover Mars with a thin film of water about 10^{-5} m thick (Jakosky and Farmer, 1982).

Enthalpy remains fairly constant at ΔH = 52.783 +/- 1.206 kJ/mol. This isolates the effects of specific surface area on regolith-driven adsorption. Particle size distribution (PSD) can be used to determine the exposure of soil to liquid water. The result of which is usually indicative of chemical alteration (*i.e.* aqueous interactions), rather than mechanical processes. (Pike *et al.*, 2011). A further investigation at the Phoenix landing site goes on to describe the regolith as being a well-mixed material with a grain size distribution comprised of large, rounded grains and small reddish fines, with a notably low mass proportion in the clay-size range below 2 μm (Pike *et al.*, 2011). Disregarding the likelihood of large percentages of clays like montmorillonite comprising regolith at the Phoenix landing site, materials like basalts, ferrihydrite, and perchlorates become more realistic when modeling the Martian regolith (Hecht

et al., 2009; Smith *et al.*, 2009) under this PSD regime. With an ideal adsorption coefficient, C = 89.4, and ideal specific surface area, SSA = 1.7 x 10^4 m^2/kg, we conclude that the regolith at the Phoenix landing site is most likely a mixture of palagonitic material (Feldman *et al.*, 2002), with properties similar to JSC-Mars 1 used in the model, likely of volcanic or basaltic origin, as well as dunite and ferrihydrite; the distribution of which is well mapped by the Mars Express OMEGA instrument and has been shown to control the atmospheric relative humidity (Pommeral *et al.*, 2009; Poulet *et al.*, 2007; Jakosky *et al.*, 2005; Smith *et al.*, 2002). We conclude that the water content in the regolith at the Phoenix landing site and thus, adsorption is driven by localized, diurnal variations in the relative humidity.

References

Arvidson, R. E., R. G. Bonitz, M. L. Robinson, J. L. Carsten, R. A. Volpe, A. Trebi-Ollennu, M. T. Mellon, P. C. Chu, K. R. Davis, J. J. Wilson, A. S. Shaw, R. N. Greenberger, K. L. Siebach, T. C. Stein, S. C. Cull, W. Goetz, R. V. Morris, D. W. Ming, H. U. Keller, M. T. Lemmon, H. G. Sizemore, M. Mehta (2009) Results from the Mars Phoenix lander robotic arm experiment. *Journal of Geophysical Research* 114.

Bandfield, J., Global mineral distribution on Mars (2002) *Journal of Geophysical Research: Planets* 107.

Banin, A. and J. Rishpon, Smectitie clays in Mars soil: Evidence for their presence and role in Viking biology experimental results (1979) *Journal of Molecular Evolution* 14, 1-3, 133-152.

Beck, P., A. Pommerol, B. Schmitt, O. Brissaud (2010) Kinetics of water adsorption on minerals and the breathing of the Martian regolith. *Journal of Geophysical Research* 115.

Bibring, J-P., Y. Langevin, J. F. Mustard, F. Poulet, R. Arvidson, A. Gendrin, B. Gondet, *et al*. (2006) Global mineralogical and aqueous Mars history derived from OMEGA/Mars Express data. *Science* 312. 5772. 400-404.

Boynton, W. V., W. C. Feldman, S. W. Squyres, and T. H. Prettyman, Distribution of hydrogen in the near surface of Mars: Evidence for subsurface ice deposits (2002) *Science*, 297, 81-85.

Bruch, L. W., M. W. Cole, and E. Zaremba, Physical adsorption: Forces and phenomena (1997) *International Series of Monographs on Chemistry* 33, Clarendon: New York, 340 pp. ISBN 0-19-855638-1.

Brunauer, S., P. H. Emmett, E. Teller (1938) Adsorption of gases in multimolecular layers. *Journal of the American Chemical Society* 60, 309-319.

Bryson, K. L., V. F. Chevrier, D. W. G. Sears, R. Ulrich (2008) Stability of ice on Mars and the water vapor diurnal cycle: Experimental study of the sublimation of ice through a fine-grained basaltic regolith. *Icarus* 196, 446-458.

Chevrier, V. F., D. R. Ostrowski, D.W. G. Sears (2008) Experimental study of the sublimation of ice through an unconsolidated clay layer: Implications for the stability of ice on mars and the possible diurnal variations in atmospheric water. *Icarus* 196, 459-476.

Chevrier, V. F., D. R. Ostrowski, and D. W. G. Sears, Experimental study of the sublimation of ice through an unconsolidated clay layer: Implications for the stability of ice on Mars and the possible diurnal variations in atmospheric water (2008) *Icarus*, 196, 459-476.

Chevrier, V. F. and T. S. Altheide, Low temperature aqueous ferric sulfate solutions on the surface of Mars (2008) *Geophysical Research Letters*, 35.

Chevrier, V. F., J. Hanley, and T. S. Altheide, Stability of perchlorate hydrates and their liquid solutions at the Phoenix landing site, Mars (2009) *Geophysical Research Letters*, 36.

Christensen, P. R., J. L Bandfield, J. F. Bell III, N. Goelick, V. E. Hamilton, A. Ivanov, B. M. Jakosky, H. H. Kieffer, M. D. Lane, M. C. Malin *et al.*, Morphology and composition of the surface of Mars: Mars Odyssey THEMIS results (2003) *Science* 300, 5628, 2056-2061.

Christensen, P. R., B. M. Jakosky, H. H. Kieffer, M. C. Malin, H.Y. McSween Jr., K. Nealson, G. L. Mehall, S. H. Silverman, S. Ferry, M. Caplinger, and M. Ravine, The Thermal Emission Imaging System (THEMIS) for the Mars 2001 Odyssey mission (2004) *Space Science Reviews* 110, 1-2, 85-130.

Clark, B. C. and D. C. Van Hart, The salts of Mars (1981) *Icarus* 45, 2, 370-378.

Coleman, N. M. and V. R. Baker, Surface morphology and origin of outflow channels in Valles Marineris region (2009) Megaflooding on Earth and Mars. *Cambridge University Press*.

Cull, S., R. E. Arvidson, M. Mellon, S. Wiseman, R. Clark, T. Titus, R. V. Morris, and P. McGuire (2010) Seasonal H2O and CO2 ice cycles at the Mars Phoenix landing site: 1. Prelanding CRISM and HiRISE observations. *JGR: Planets*, 115, E4.

Cull, S., R. E. Arvidson, R. V. Morris, M. Wolff, M. T. Mellon, and M. T. Lemmon (2010) Seasonal ice cycle at the Mars Phoenix landing site: 2. Postlanding CRISM and ground observations. *JGR: Planets*, 115, E5.

Feldman,W. C., W. V. Boynton, R. L. Tokar, T. H. Prettyman, O. Gasnault, S. W. Squyres, R. C. Elphic, D. J. Lawrence, S. L. Lawson, S. Maurice, G. W. McKinney, K. R. Moore, and R. C. Reedy (2002) Global distribution of neutrons from Mars: Results from Mars Odyssey. *Science* 297, 4479, 75-78.

Haberle, R. M., C. P. McKay, J. Schaeffer, N. A. Cabrol, E. A. Grin, A. P. Zent, and R. Quinn, On the possibility of liquid water on present-say Mars (2001) *Journal of Geophysical Research: Planets*, 106.

Head, J. W., A. L. Nahm, D. R. Marchant, and G. Neukum, Modification of the dichotomy boundary on Mars by Amazonian mid-latitude glaciation (2006) *Geophysical Research Letters*, 33.

Hecht, M. H., Metastability of liquid water on Mars (2002) *Icarus*, 156, 373-386.

Hecht, M. H., S. P. Kounaves, R. C. Quinn, S. J. West, S. M. M. Young, D. W. Ming, D. C. Catling, B. C. Clark, W. V. Boynton, J. Hoffman, L. P. DeFlores, K. Gospodinova, J. Kapit and P. H. Smith (2009) Detection of perchlorate and the soluble chemistry of martian soil at the Phoenix landing site. *Science,* 325 (5936), 64-47.

Huguenin, R. L., Chemical weathering and the Viking Biology Experiments on Mars (1982) *Journal of Geophysical Research: Solid Earth* 87, B12, 10069-10082.

Jakosky, B. M. and C. B. Farmer (1982) The seasonal and global behavior of water vapor in the Mars atmosphere: Complete global results of the Viking Atmospheric Water Detector Experiment. *Journal of Geophysical Research: Solid Earth*, 87, B4, 2999-3019.Jakosky, B. M., M. T. Mellon, E. S. Varnes, W. C. Feldman, W. V. Boynton, R. M. Haberle (2005) Mars low-latitude neutron distribution: Possible remnant near-surface water ice and a mechanism for its recent emplacement. *Icarus* 175, 58-67.

Kournaves, S. P., N. A. Chaniotakis, and V. F. Chevrier, Identification of the perchlorate parent salts at the Phoenix landing site and possible implications (2014) *Icarus*, 232, 226-231.

Langmuir, I., The adsorption of gases on plane surfaces of glass, mica, and platinum (1918) *Contribution from the Research Laboratory of the General Electric Company*, 1361-1403.

Laskar, J., A. C. M. Correia, M. Gastineau, F. Joutel, B. Levrard, and P. Robutel, Long term evolution and chaotic diffusion of the insolation quantities of Mars (2004) *Icarus*, 170, 343-364.

Levy, J. S., Hydrological characteristics of recurrent slope lineae on Mars: Evidence for liquid flow through regolith and comparisons with Antarctic terrestrial analogs (2012) *Icarus*, 219, 1-4.

Lobitz, B., B. L. Wood, M. M. Averner, and C. P. McKay, Use of spacecraft data to derive regions on Mars where liquid water would be stable (2001) *Proceedings of the National Academy of Sciences of the United States of America*, 98.

Malin, M. C. and Edgett, K. S., Evidence for recent groundwater seepage and surface runoff on Mars (2000) *Science*, 288, 2330-2335.

Marchant, D. R. and Head, J. W., Antarctic Dry Valleys: Microclimate zonation, variable geomorphic processes, and implications for assessing climate change on Mars (2007) *Icarus*, 192, 187-222.

Mellon, M. T., R. E. Arvidson, H. G. Sizemore, M. L. Searls, D. L. Blaney, S. Cull, M. H. Hecht, T. L. Heet, H. U. Keller, M. T. Lemmon, W. J. Markiewicz, D. W. Ming, R. V. Morris, W. T. Pike, and A. P. Zent, Ground ice at the Phoenix landing site: Stability state and origin (2009) *Journal of Geophysical Research: Planets* 114, E1.

Mellon, M. T. and Jakosky, B. M., The distribution and behavior of Martian ground ice during past and present epochs (1995) *Journal of Geophysical Research: Planets*, 100.

Mitrofanov, I., D. Anfimov, A. Kozyrev, M. Litvak, A. Sanin, V. Tret'yakov, A. Krylov, V. Shvetsov, W. Boynton, C. Shinohara, D. Hamara and R. S. Saunders (2002) Maps of subsurface hydrogen from the high energy neutron detector, Mars Odyssey. *Science* 297, 78-81.

Ohja, L., M. B. Wilhelm, S. L. Murchie, A. S. McEwen, J. J. Wray, J. Hanley, M. Masse, and M. Chojnacki, Spectral evidence for hydrated salts in recurring slope lineae on Mars (2015) *Nature Geosciences*, 8, 829-832.

Pike, W. T., U. Staufer, M. H. Hecht, W. Goetz, D. Parrat, H. Sykulska-Lawrence, S. Vijendran, and M. B. Madsen (2011) Quantification of the dry history of the Martian soil inferred from in situ microscopy. *Geophysical Research Letters* 38.

Pommerol, A., B. Schmitt, P. Beck, O. Brissaud (2009) Water sorption on martian regolith analogs: Thermodynamics and near-infrared reflectance spectroscopy. *Icarus* 204, 114-136.

Poulet, F., C. Gomez, J. P. Bibring, Y. Langevin, B. Gondet, P. Pinet, G. Belluci, and J. Mustard (2007) Maritan surface mineralogy from Observatoire pour la Mineralogie, l'Eau, les Glaces et l'Activite on board the Mars Express spacecraft (OMEGA/MEx): Global mineral maps. *Journal of Geophysical Research: Planets*, 112, E8.

Rivera-Valentin, E. G. and V. F. Chevrier (2015) Revisiting the Phoenix TECP data:Implications for regolith control of near-surface humidity on Mars. *Icarus* 253, 156-158.

Sears, D. W. G. and J. D. Chittenden, On laboratory simulation and the temperature dependence of evaporation rate of brine on Mars (2005) *Geophysical Research Letters*, 32.

Sears, D. W. G. and S. R. Moore, On laboratory simulation and the evaporation rate of water on Mars (2005) *Geophysical Research Letters*, 32.

Smith, P. H., L. K. Tamppan, R. E. Arvidson, D. Bass, D. Blaney, W. V. Boynton, A. Carswell, D. C. Catling, B. C. Clark, T. Duck, E. DeJong, D. Fisher, W. Goetz, H. P. Gunnlaugsson, M. H. Hecht, V. Hipkin, J. Hoffman, S. F. Hviid, H. U. Keller, S. P. Kournaves, C. F. Lange, M. T. Lemmon, M. B. Madsen, W. J. Markiewicz, J. Marshall, C. P. McKay, M. T. Mellon, D. W. Ming, R. V. Morris, W. T. Pike, N. Renno, U. Staufer, C. Stoker, P. Taylor, J. A. Whiteway, A. P. Zent (2009) H2O at the Phoenix landing site. *Science* 325 (5936), 58-61.

Zent, A. P and R. C. Quinn (1997) Measurement of H_2O adsorption under Mars-like conditions: Effects of adsorbent heterogeneity. *Journal of Geophysical Research: Planets* 102, 9085-9095.

Zent, A. P., D. J. Howard, R. C. Quinn (2001) H_20 adsorption on smectites: Application to the diurnal variation of H_2O in the martian atmosphere. *Journal of Geophysical Research: Planets* 106, 14,667-14,674.

Zent, A. P. *et al.,* (2009) Thermal and electrical conducitivity probe (TECP) for Phoenix. *Journal of Geophysical Research: Planets* 114. E00A27.

Zent, A. P., M. H. Hecht, D. R. Cobos, S. E. Wood, T. L. Hudson, S. M. Milkovich, L. P. DeFlores, and M. T. Mellon, Initial results from the thermal and electrical conductivity probe (TECP) on Phoenix (2010) *Journal of Geophysical Research*, 115, E00E14.

Zent, A. P., M. H. Hecht, T. L. Hudson, S. E. Wood, and V. F. Chevrier, A revised calibration function and results for the Phoenix mission TECP relative humidity sensor (2016) *Journal of Geophysical Research: Planets*, 121. 4, 626-651.

Zorzano, M. -P., E. Mateo-Martí, O. Prieto-Ballesteros, S. Osuna and N. Renno, Stability of liquid saline water on present day Mars (2009) *Geophysical Research Letters*, 36, 2.